Mineral Transformations in Gold–(Silver) Tellurides in the Presence of Fluids: Nature and Experiment

Jing Zhao * [iD] **and Allan Pring**

Chemical and Physical Sciences, College of Science and Engineering, Flinders University, Bedford Park, Adelaide, SA 5042, Australia; allan.pring@flinders.edu.au
* Correspondence: jing.zhao@flinders.edu.au

Abstract: Gold–(silver) telluride minerals constitute a major part of the gold endowment at a number of important deposits across the globe. A brief overview of the chemistry and structure of the main gold and silver telluride minerals is presented, focusing on the relationships between calaverite, krennerite, and sylvanite, which have overlapping compositions. These three minerals are replaced by gold–silver alloys when subjected to the actions of hydrothermal fluids under mild hydrothermal conditions ($\leq$220 °C). An overview of the product textures, reaction mechanisms, and kinetics of the oxidative leaching of tellurium from gold–(silver) tellurides is presented. For calaverite and krennerite, the replacement reactions are relatively simple interface-coupled dissolution-reprecipitation reactions. In these reactions, the telluride minerals dissolve at the reaction interface and gold immediately precipitates and grows as gold filaments; the tellurium is oxidized to Te(IV) and is lost to the bulk solution. The replacement of sylvanite is more complex and involves two competing pathways leading to either a gold spongy alloy or a mixture of calaverite, hessite, and petzite. This work highlights the substantial progress that has been made in recent years towards understanding the mineralization processes of natural gold–(silver) telluride minerals and mustard gold under hydrothermal conditions. The results of these studies have potential implications for the industrial treatment of gold-bearing telluride minerals.

1. Introduction

Gold–(silver) tellurides are important accessory minerals, carrying a significant proportion of the gold endowment in some low to medium temperature hydrothermal vein deposits. Gold–(silver) telluride minerals have become one of the most important sources of gold in the world. The Golden Mile deposit in Kalgoorlie, Western Australia, has been an economically important gold–(silver) telluride deposit for over a century; it contained approximately 1450 tons gold, of which approximately 20% was in the form of tellurides [1]. Other notable modern and historic gold deposits carrying significant amounts of the gold as tellurides include Cripple Creek, Colorado (~875 tons gold) [2]; Emperor, Fiji (~360 tons of gold, 10–50% occurring as tellurides) [3,4]; and Săcărîmb, Romania [5]. Another important example is the recently discovered Sandaowanzi gold deposit on the northeastern edge of the Great Xing'an Range, Heilongjiang Province, North East China, with a total reserve of $\geq$25 tons of gold and an average grade of 15 g/t [6–9]. We believe that this is the first case of a major gold deposit in which the gold telluride minerals are the dominant ore, with more than 95% of recovered gold occurring as tellurides.

Eight gold–(silver) tellurides have been described and are currently recognized as valid minerals: calaverite, krennerite, sylvanite, petzite, muthmannite, empressite, hessite, and stuetzite. A summary

of the characteristics and physical properties of the main gold (and/or silver) telluride minerals is presented in Table 1 and the compositions of these minerals are shown in Figure 1. The gold-rich telluride species—calaverite, krennerite and sylvanite—are the most common and economically important minerals of the group, with a chemical composition of $Au_{1-x}Ag_xTe_2$. Cabri [10] gave the following compositional fields for these minerals: Calaverite 0 to 2.8 wt % Ag ($0 \leq x \leq 0.11$); krennerite 3.4 to 6.2 wt % Ag ($0.14 \leq x \leq 0.25$); and sylvanite 6.7 to 13.2 wt % Ag ($0.27 \leq x \leq 0.50$). A more recent work by Bindi et al. [11] showed that calaverite and sylvanite can have overlapping compositional fields, and share a similar layered structural topology (as shown in Figure 2). The Ag content of calaverite, sylvanite, and krennerite has been linked to its substitution for Au and stabilization of the complex modulated structures adopted by these minerals [11,12]. The incommensurately modulated structure of calaverite was determined by Bindi et al. [11] and its modulations are related to the distribution of Au^{3+} and Au^+ and the substitution of Ag^+ for Au^+. In krennerite, Ag and Au are ordered to avoid Ag–Te–Ag linkages [12]. Sylvanite occurs in two forms, one is a commensurately modulated superstructure based on the calaverite sub-cell and the other is an incommensurately modulated form [13]. On a historical note, calaverite was the first mineral, or compound, to be recognized to have an incommensurately modulated structure. It was identified by morphological crystallographers in 1901 as their attempts to index crystal faces required a model which had intergrowing lattices [14]. The other five telluride minerals listed in Table 1 are much less important in gold production and four of them contain more silver than gold.
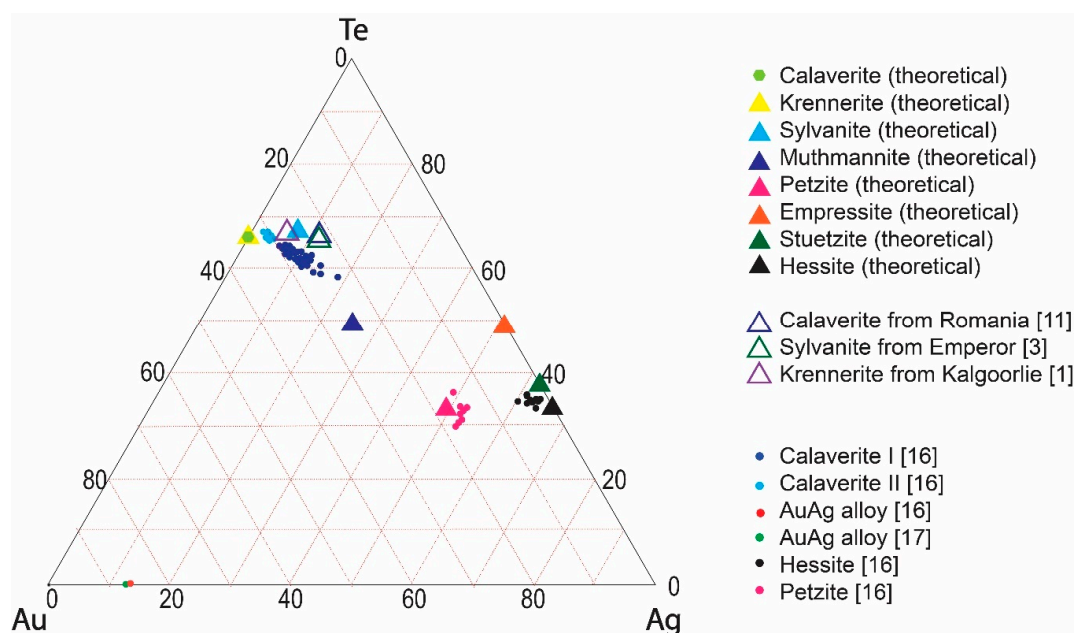

Figure 1. Ternary diagrams of Au–(Ag)–Te system (atom%), showing compositions of gold–(silver) tellurides from mineral database [15] and references [1,3,8,11,16,17]. Compositions of synthetic gold–(silver) tellurides [16,17] are shown as small colored dots.

Gold–(silver) telluride minerals in gold deposits are considered refractory ores from a mineral processing perspective, as they are not efficiently leachable in cyanide solutions. Therefore, additional processing steps are required to improve gold recovery when tellurides are present in the ore (e.g., [18,19]). Fine grinding and pretreatments (normally roasting gold tellurides at temperatures ≥800 °C) are generally utilized to improve gold recovery. These methods are energy-intensive and raise environmental issues due to the release of Te species into the atmosphere. An alternative strategy for gold recovery from telluride ores is needed for deposits rich in these refractory gold ores.
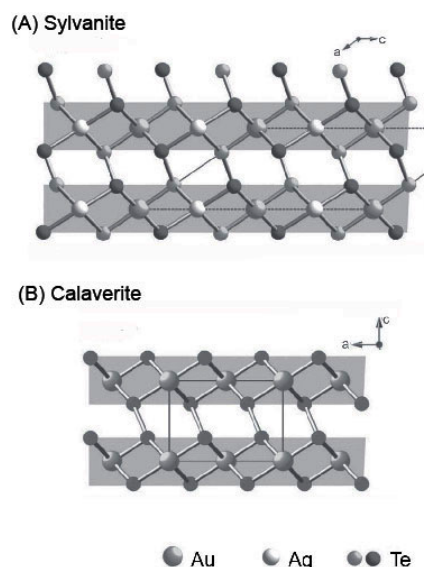
Figure 2. Projections of the crystal structures of sylvanite (**A**) and calaverite (**B**). Crystal structure data for the minerals are from references [11,20].

Table 1. Characteristics and physical properties of the main gold–(silver) tellurides.

Mineral	Chemical Formula	Color	Density (g/cm^3)	Hardness	Composition wt %		
					Au	Ag	Te
Calaverite	$AuTe_2$	Silver white to brassy yellow	9.04	2.5–3	43.6	0	56.4
Krennerite	$(Au_{1-x},Ag_x)Te_2$	Silver white to blackish yellow	8.53	2.5	43.6	0	56.4
Sylvanite	$AuAgTe_4$	Steely gray to silver gray	7.9–8.3 (8.1)	1.5–2	34.4	6.3	59.4
Muthmannite	$(Ag,Au)Te_2$	Blackish yellow, grayish white	-	2.5	34.3	19.2	46.5
Petzite	Ag_3AuTe_2	Bright steel gray to iron black	8.7–9.14	2.5	25.4	41.7	32.9
Empressite	$AgTe$	Bronze, light bronze	7.5–7.6	3.5	0	46.3	53.7
Stuetzite	$Ag_{5-x}Te_3$, (x = 0.24–0.36)	Gray, dark bronze	8	3.5	0	57.0	43.0
Hessite	Ag_2Te	Lead gray, steel gray	7.2–7.9	1.5–2	0	62.8	37.2

Note: Data is from [15].

2. Gold–(Silver) Tellurides in Nature and Their Alteration

The economic importance of gold–(silver) telluride minerals in gold deposits has meant that they have received significant attention from geologists and mineralogists. More than 100 occurrences have been reported worldwide. The International Geoscience Programme project IGCP-486 was undertaken from 2003 to 2008 and focused on the interplay between mineralogy and ore genesis of telluride minerals [4]. The project directly contributed to a summary of the distribution of gold–(silver) telluride-bearing deposits and a better understanding of the formation of these deposits. Gold–(silver) telluride deposits normally contain a dozen or more different telluride and selenide minerals and present complex ore textures. An example is seen in the ores of the recently discovered Sandaowanzi gold deposit, where sylvanite is the most abundant gold-bearing mineral and together with petzite and krennerite accounts for >60% of the total tellurides by volume [7,8]. The mixtures of gold–(silver) telluride minerals were explored in both vein ores and disseminated ores [7]. As shown in Figure 3, gold and krennerite coexist with petzite and stuetzite, or form symplectic intergrowths with sylvanite. The size of individual telluride grains at this deposit can be up to 3 cm in diameter. In these textures (Figure 3A), stuetzite is irregularly shaped and randomly distributed as patches within petzite symplectites. Native gold and krennerite occur in close association as a mineral pair and are often included within petzite–stuetzite symplectites. Native gold also occurs as isolated grains along intragranular cracks in the telluride grains. The various combinations of gold tellurides (Figure 3B) have been attributed to retrograde reactions [21], and Liu et al. [8] suggested the formation of telluride assemblages at Sandaowanzi is related to the breakdown of early telluride phases (e.g., γ-phase and χ-phase of Cabri [10]). In this deposit, isolated gold grains occur in a "bamboo shoot-like" morphology

(Figure 3C), with the filaments being 3 to 5 μm in diameter and 10 to 15 μm in length. Gold also occurs in irregular patches within cavities in gold tellurides (Figure 3D).
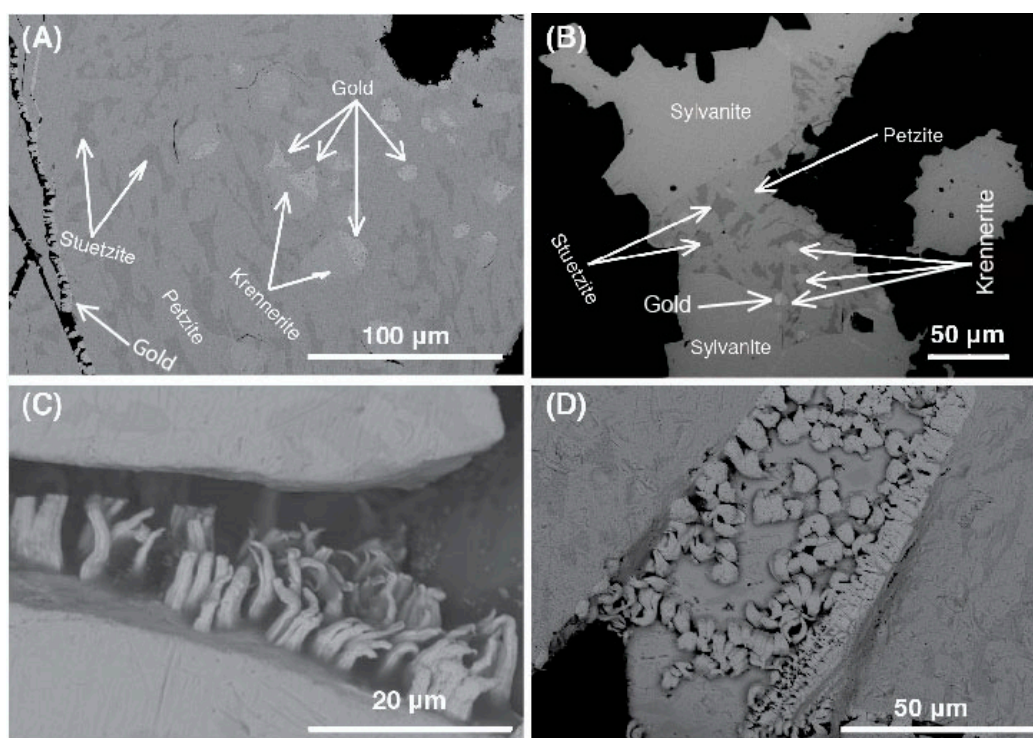

Figure 3. Mineralogy and microstructures of Au–(Ag) telluride ores at Sandaowanzi deposit [7,8]. (**A**) Native gold along intragranular cracks in the telluride grains and native gold–krennerite pair included in petzite–stuetzite symplectite. (**B**) Native gold and krennerite patches contained a petzite–stuetzite symplectite in association with sylvanite. (**C**) Bamboo shoot-like native gold grains along intragranular cracks in telluride grains. (**D**) Irregular shaped native gold grains within a cavity in gold tellurides.

The alteration of gold–(silver) tellurides to fine wires, or spongy gold, is well known [22] and the gold product is sometimes called "mustard gold" because of its distinctive appearance in reflected light (Figure 4) [23]. The formation of mustard gold at the Dongping Mines (Hebei Province, China) has been linked to the decomposition of calaverite by selective leaching of tellurium while leaving the gold alloy in the cavity formed by the alteration reaction [24,25]. This type of pseudomorphic alteration was also documented by Palache et al. [26]. The occurrence of microporous gold has also been observed under cold climatic conditions, such as at the Aginskoe low-sulfidation epithermal deposit in Central Kamchatka, Russia. In this deposit, calaverite is the main Au telluride mineral and it has been partially replaced by porous gold [27]. By comparing the textures of microporous gold from this natural occurrence with those obtained experimentally via the dealloying of gold–(silver) tellurides [16,17,28,29], Okrugin et al. [30] confirmed that natural microporous gold can form via the replacement of telluride minerals and assessed the role that hydrothermal fluids may play in the formation of microporous gold.
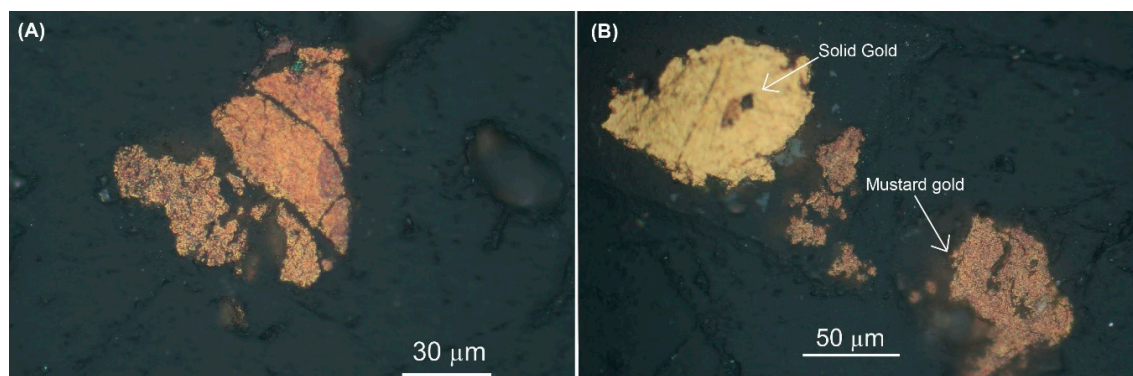
Figure 4. Native gold from the Gaching ore occurrence (Maletoyvayam ore field), Kamchatka, Russia (polished sections in reflected light) (imaged by N. Tolstykh). (**A**) Color of mustard gold is brown yellow to brown under reflected light. (**B**) Porous gold (mustard gold) is observed along with a homogeneous gold grain (solid gold).

3. Mineral Replacement Reactions of Gold–(Silver) Tellurides in the Presence of Fluids

There are limited reliable thermodynamic data for gold–(silver) tellurides due to the compositional overlap and structural complexity of the main mineral phases and therefore the difficulty in calculating meaningful phase diagrams that represent observed assemblages in Au–Ag–Te systems. Many studies on tellurium-bearing systems have focused only on the binary subsystems of Au–Te and Ag–Te. Since the 1960s, several experimental [10,31,32] and theoretical studies (e.g., [33]) have been conducted on the Au–Ag–Te system. Cabri [10] conducted a systematic investigation in the Au–Ag–Te ternary system, to determine the equilibrium phase relations in the mineralogically important area of the ternary system and phase changes in the assemblages over a range of temperatures. However, it should be noted that Cabri's study was performed using traditional dry sealed tube methods rather than under hydrothermal conditions. Zhang et al. [34] evaluated the stability of calaverite and hessite and discussed it in the context of the stability of other minerals in the Au–Ag–Te system. The calculated stability of hessite and calaverite were used to explain the physicochemical conditions of formation of the Gies and Golden Sunlight gold–(silver) telluride deposits in Montana, USA. Wang et al. [35] contributed new thermodynamic data for the Au–Te system, while McPhail [36] and Grundler et al. [37–39] studied the complexation and transport of tellurium in hydrothermal fluids.

The mineral replacement reactions of gold–(silver) tellurides in the presence of fluids have been explored in recent years. In a study of the kinetics and mechanism of mineral replacement reactions, Zhao et al. [28] investigated the replacement of calaverite by porous gold over a wide range of hydrothermal conditions. The transformation proceeds in a pseudomorphic manner via a coupled dissolution-reprecipitation (CDR) reaction mechanism. While the gold precipitates locally and preserves the shape of the original calaverite grain, the tellurium is selectively removed and lost to the bulk solution. Zhao et al. [16] further investigated the transformation of sylvanite to Au–Ag alloy by exploring the roles of temperature and fluid composition. The reaction follows a complex path, where CDR reactions interact with solid-state diffusion processes, and results in complex textures. This complexity is due to the fact that sylvanite has a higher Ag content, which results in the formation of a metastable Ag-rich, Te-depleted calaverite I phase. To achieve equilibrium, the metastable phase breaks down to stable calaverite II plus phase-χ. Phase-χ subsequently breaks down to hessite and petzite. To further investigate the effects of Ag in the parent crystal for the reaction path of Au–Ag tellurides during replacement, Xu et al. [17] designed a set of hydrothermal experiments using krennerite under similar conditions to those used by Zhao et al. [16,24]. The results show that krennerite transformed to Au–Ag alloy in a pseudomorphic manner very similar to calaverite and distinct from sylvanite. The reaction paths of these three reactions are summarized in Figure 5. In the next section we will review in detail these three comprehensive studies of the transformation of

calaverite, krennerite, and sylvanite to gold–silver alloys by CDR reactions, focusing on the product textures, reaction mechanism, and the kinetics of the oxidative leaching of Te.
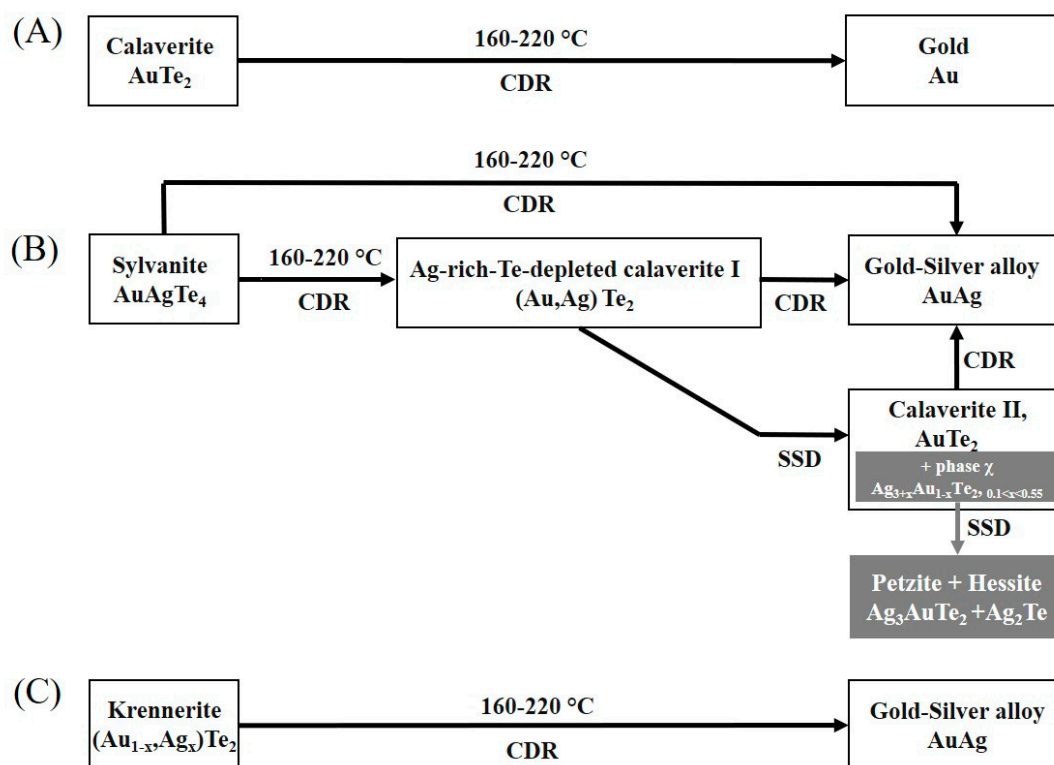

Figure 5. Overview of the proposed reaction paths of the hydrothermal reaction for calaverite (**A**), sylvanite (**B**) and krennerite (**C**). CDR stands for coupled dissolution reprecipitation and SSD stands for solid state diffusion.

3.1. Product Textures

When calaverite grains are heated in a series of 0.2 M buffer solutions (ranging from $pH_{25\,°C}$ 2 to 12) at 220 °C, Te is selectively removed from the calaverite, leaving a rim of porous gold (Figure 6A) [28]. The gold filaments produced grow perpendicular to the surface of calaverite. The gold filaments have diameters ranging from 200 to 500 nm, with lengths up to ~25 μm (Figure 6B). Texturally, they are randomly-oriented gold crystals, forming generally dendritic aggregates (Figure 6C). This texture is most likely due to repeated twinning on {111}, which is common in reticulated and dendritic gold aggregates [26]. The morphology of the gold sponge does not vary significantly with solution pH and temperature, but the extent of the reaction depends on the solubility of Te^{4+} in solution, and this is pH-dependent (Figure 7) [28,39]. The textural features of the replacement of calaverite by gold are consistent with a pseudomorphic replacement reaction proceeding via an interface-coupled dissolution reprecipitation (ICDR) process [40–42].
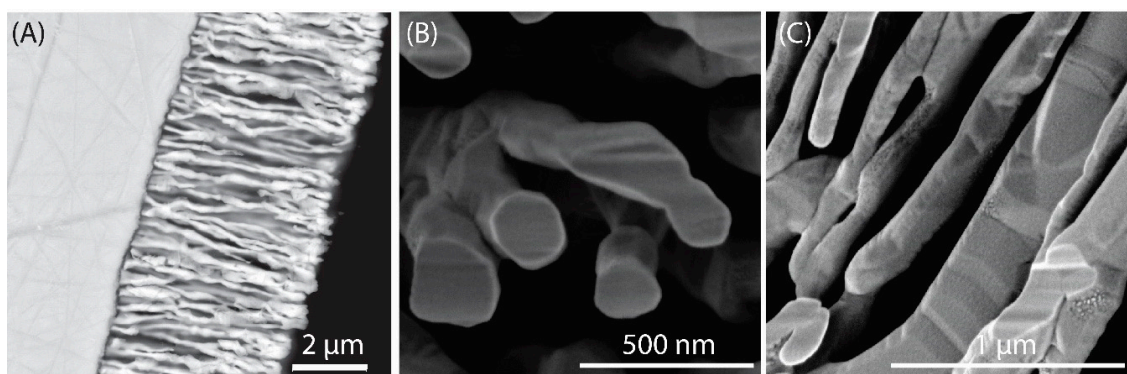
Figure 6. (**A**) Back-scattered electron image of cross section of partially-reacted calaverite showing the phase boundary between the porous gold product and the parent calaverite (solid grain). High-magnification images of gold showing three-dimensional structure of gold filaments, which were cut perpendicular (**B**) and parallel (**C**) to the long axis of the gold filaments.
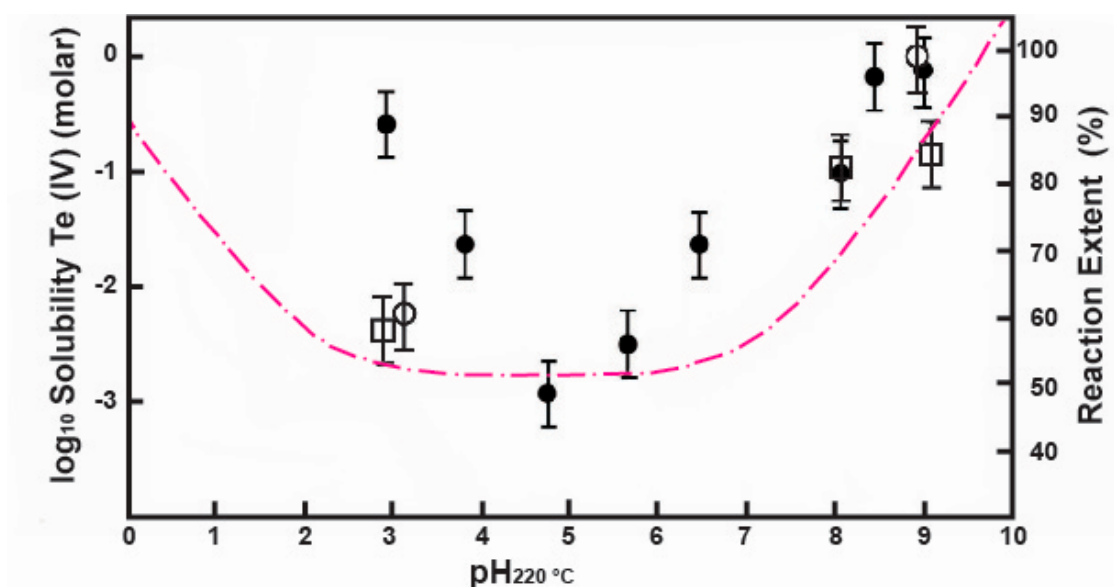

Figure 7. The curve of estimated solubility of Te(IV) in water at 220 °C is shown as pink dashed line (data from reference [28,38,39]). Solid circles stand for the reaction extent of the replacement of calaverite [28]. Hollow circles and squares stand for the replacement of krennerite [17] and sylvanite [16], respectively. Errors of the reaction extent ($3 - \sigma$; $\pm$ 6%) are plotted at each point. Reaction extent observed experimentally corresponded well to the solubility of tellurium.

The replacement of krennerite is similar to calaverite [17], proceeding via the ICDR reaction mechanism. An Au–Ag alloy of wormlike filaments was produced due to higher silver contents in krennerite (Figure 8). Natural krennerite normally contains 3.4 to 6.2 wt % Ag ($0.14 \leq x \leq 0.25$), compared to calaverite which contains 0 to 2.8 wt % Ag ($0 \leq x \leq 0.11$) [10]. The krennerite used in a study by Xu et al. [17] had a composition $Au_{0.82}Ag_{0.18}Te_{2.00}$, and an Au:Ag ratio of 4.6. The average composition of the product is $Au_{0.85}Ag_{0.15}$, and Au:Ag is ~5.7, which is slightly higher than that of the parent krennerite. The increase of the Au:Ag ratio is due to the dissolution of Ag in the reaction fluid and in textural terms for the Au–Ag alloy filaments have diameters ranging from 200 to 1000 nm. As the reaction proceeds, Au–Ag alloy wires also develop locally, having diameters up to 5 μm and lengths ranging from 25 μm to 200 μm and longer.
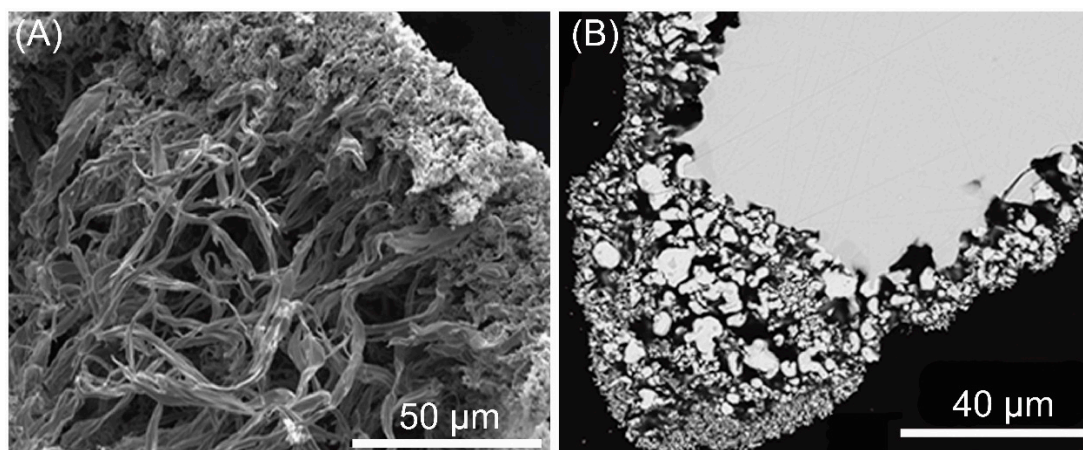
Figure 8. (**A**) Secondary electron image showing the highly porous Au–Ag alloy in the shape of filaments. (**B**) Backscattered electron image of cross section of partially-reacted krennerite grains showing larger Au–Ag alloy particles coexisting with fine-grained Au–Ag alloy in the resultant gold rim (imaged by W. Xu).

Compared to calaverite and krennerite, sylvanite generally contains significantly higher Ag contents (6.7 to 13.2 wt % Ag, illustrated by Cabri [10]). In the study by Zhao et al. [16] the sylvanite had a composition of $Au_{0.63}Ag_{0.36}Te_{2.00}$ which corresponds to 9.2 wt % Ag. In contrast to the replacement of calaverite and krennerite, sylvanite was replaced by an assemblage of products and the resulting textures are complex. In addition to Au–Ag alloy ($Au_{0.87}Ag_{0.13}$), a range of other phases formed as intermediate products, including petzite (($Au_{0.92}Ag_{3.15}$)Te_2), hessite ($Ag_{1.89}Au_{0.07}Te$), and two compositions of calaverite. The calaverite I phase has an Ag-rich, Te-depleted composition, ($Au_{0.78}Ag_{0.22}$)$Te_{1.74}$, which is similar to natural krennerite, but its XRD pattern is close to natural calaverite. Calaverite II has a normal calaverite composition of ($Au_{0.93}Ag_{0.07}$)Te_2. The calaverite I phase is porous while calaverite II lacks obvious signs of porosity in SEM images. The texture of a partially-reacted sylvanite grain is shown in Figure 9. The Au–Ag alloy rim is composed of wormlike Au–Ag alloy particles (Figure 9A), with diameters ranging from 200 to 1000 nm. Wire gold has also developed locally (up to 5 µm in diameter, 25 µm in length; Figure 9A). The rim of the grain is highly porous, with the Au–Ag alloy growing loosely on the surface and along cracks within the sylvanite (Figure 9B). Relatively large gaps were observed between the alloy rim and the particle. Underneath the Au–Ag alloy rim (Figure 9C,D), sylvanite is replaced by assemblages of calaverite I and a mixture of petzite and hessite. Petzite and hessite occur intimately mixed either as small patches or inclusions within calaverite I, or adjacent to grains of calaverite II. Au–Ag alloy and calaverite II are observed together within petzite-hessite lamellae, which is similar to the textures of natural tellurides at the Sandaowanzi deposit.
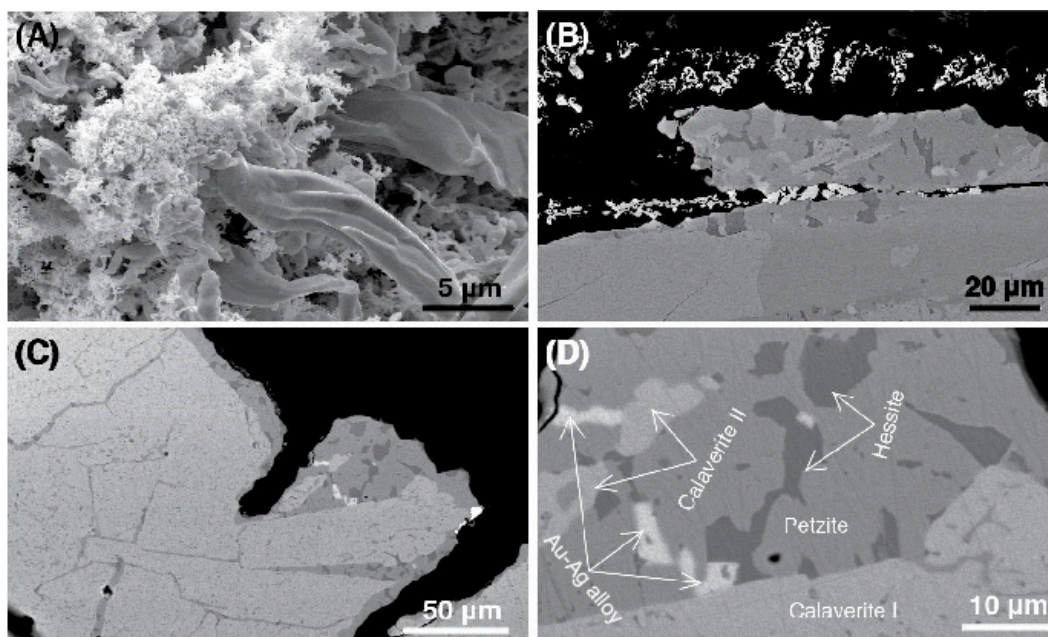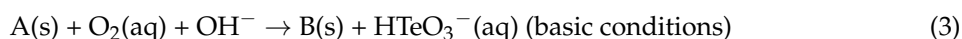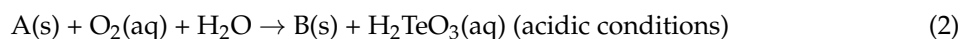
Figure 9. (**A**) Secondary electron images showing the micro Au–Ag alloy wires growing on the surface of a partially-reacted sylvanite grain. (**B,C**) Backscattered electron images of cross section of partially-reacted sylvanite grains showing a range of products after the replacement reaction. (**D**) Zoomed in image of Figure 9C, showing the textures of the calaverite II, petzite, hessite, and Au–Ag alloy; petzite and hessite occur intimately mixed either as small patches or inclusions within calaverite I.

3.2. Reaction Mechanism

Under oxidizing conditions, gold–(silver) tellurides are ultimately replaced by gold or Au–Ag alloy, while the Te is eventually lost to bulk solution and some is precipitated in the form of $TeO_2(s)$ particles on the outer surface of gold/Au–Ag alloy. The selective removal of Te from gold–(silver) tellurides is often referred to as leaching, a process conventionally considered as a solid-state diffusion-driven mechanism. In this case, it proceeds in a pseudomorphic manner via an interface-coupled dissolution–reprecipitation (ICDR) mechanism (summarized in Figure 10). The distinctive textural outcome of a CDR reaction is that the product phase of gold or Au–Ag alloy preserves the external dimension of the parent mineral. The scale of pseudomorphism in the replacement of gold–(silver) tellurides by gold or Au–Ag alloy varies from nanometer scale (e.g., the replacement of calaverite) to a few micrometers (e.g., the replacement of sylvanite). The textural features indicate that the dissolution of gold–(silver) telluride is the rate-controlling step, which is closely coupled with the precipitation rate of the products in both space and time scales [40]. The coupling between parent and product minerals is controlled by the solution chemistry at the reaction front. The porosity is strong textural evidence for a CDR reaction. The reaction is sustained by continuous mass transport through open pathways for the influx of fluid and solutes (e.g., the oxidant) to the reaction interface and the removal of dissolved Te and Ag from the reaction interface (e.g., [43,44]). The abundant porosity of the product phases is associated with negative volume changes; although systems with positive volume changes still exhibit porosity, it is often very fine grained [45]. The overall volume change is determined by the changes in molar volume as well as the solubility of the parent and product phases within a given solution [46]. The former parameter plays a role in the extent of the volume change, but the latter determines the sign of the volume change [41,47]. The solubility of each phase is a function of the grain size, fluid composition, temperature, and pressure, among other variables, and hence will likely evolve as the replacement reaction proceeds [47]. Pollok et al. [46] defined the change in volume by considering not only molar volumes but the relative solubilities of the parent and product:

$$\Delta V = 100 \times \left(\frac{n_p V_{m,p} - n_d V_{m,d}}{n_d V_{m,d}} \right),\tag{1}$$

where n_p and n_d are the number of moles of the product precipitated and the parent dissolved, and $V_{m,p}$ and $V_{m,d}$ are the molar volumes of the precipitating and dissolving phases. Considering that metallic gold or Au–Ag alloy is the final product of the replacement reaction, the molar volume changes (ΔV) in the three replacement reactions range from −79% to −85% (details are listed in Table 2). The processes include (i) the dissolution of gold–(silver) tellurides, (ii) the oxidation of the Te to a soluble Te(IV) complex and the transportation of Te from the reaction front to the bulk hydros solution, and (iii) the precipitation of gold/Au–Ag alloy. When natural gold–(silver) tellurides are treated with solution, the dissolution of the mineral occurs at the reaction front, resulting in the formation of aqueous Au, Ag, and Te complexes. To decide the nature of the predominant aqueous species of Au, Ag, and Te, and discuss the relative solubilities of each element as a function of pH, Zhao et al. [16] calculated simple diagrams of $\log fO_2(g)$ vs. pH for the system containing the same amounts of Au, Ag, and Te added to the solution by the dissolution of sylvanite at 200 °C for a solution containing 0.01 M chloride. The results illustrate that the dominant Te aqueous species is $H_2TeO_3(aq)$ under acidic to slightly basic (pH$_{200\,°C}$ 2–7) conditions and $HTeO_3^-$ under more basic conditions. Ag is mainly present as AgCl(aq) under acidic conditions, but the dominant Ag aqueous species is $Ag(OH)_2^-$ under basic conditions. Taking $O_2(aq)$ as the oxidant and assuming Au immobility, the overall reaction of gold tellurides to Au–Ag alloy can be described as below:

$$A(s) + O_2(aq) + H_2O \rightarrow B(s) + H_2TeO_3(aq) \text{ (acidic conditions)}\tag{2}$$

$$A(s) + O_2(aq) + OH^- \rightarrow B(s) + HTeO_3^-(aq) \text{ (basic conditions)}\tag{3}$$

where A is the parent phase of gold–(silver) tellurides, and B is the solid product phase or phases. In the replacements of calaverite and krennerite, B represents the single product of gold or Au–Ag alloy. In transformation of sylvanite, B represents both calaverite I and the Au–Ag alloy. Once the concentrations of Te and Ag in solution reach a critical state, the reaction switches and sylvanite dissolution is coupled to the precipitation of calaverite I. This indicates that this reaction is controlled by the amount of Te and Ag in solution. Calaverite I is an unstable phase, which further breaks down to calaverite II and phase χ ($Ag_{3+x}Au_{1-x}Te_2$, 0.1 < x < 0.55) via exsolution which may be fluid-catalyzed [48]. Both products of calaverite and phase χ subsequently transform to Au–Ag alloy by Reactions 2 or 3. Phase χ breaks down to a fine intergrowth of petzite and hessite during the quenching of the autoclaves from the reaction temperature (160 to 220 °C) to room temperature [16]. Cabri [10] reported that phase χ breaks down to a mixture of petzite and hessite at 105 °C. It is unclear whether the breakdown of calaverite I to calaverite II plus phase χ is really a solid-state diffusion-controlled reaction, or a fluid-catalyzed breakdown reaction in which the highly porous calaverite I undergoes a recrystallization and unmixing reaction driven by a reduction of internal surface area. The lack of porosity in the calaverite II points to solid-state exsolution. Such reactions have recently been studied in the breakdown of the bornite–digenite solid solution [48,49]. Zhao et al. [50] synthesized bornite–digenite solid solution (*bdss*) by replacing chalcopyrite under hydrothermal conditions. The results demonstrated that its composition principally depended on the temperature of the reaction rather than solution composition. Upon quenching, the unquenchable nanoscale porosity within the *bdss* system coalesces into fluid inclusions, specifically along grain boundaries, which catalyze the breakdown of the unstable *bdss* to exsolve digenite [48] or chalcopyrite [49], depending on the solution condition.

The transformation of sylvanite proceeds by a complex pathway combining dissolution–reprecipitation, fluid-catalyzed unmixing, and solid-state processes, which all compete during different stages of the reaction. The interplay of different reaction mechanisms results in complex textures, which could easily be misinterpreted in terms of complex multi-episodic geological evolution.
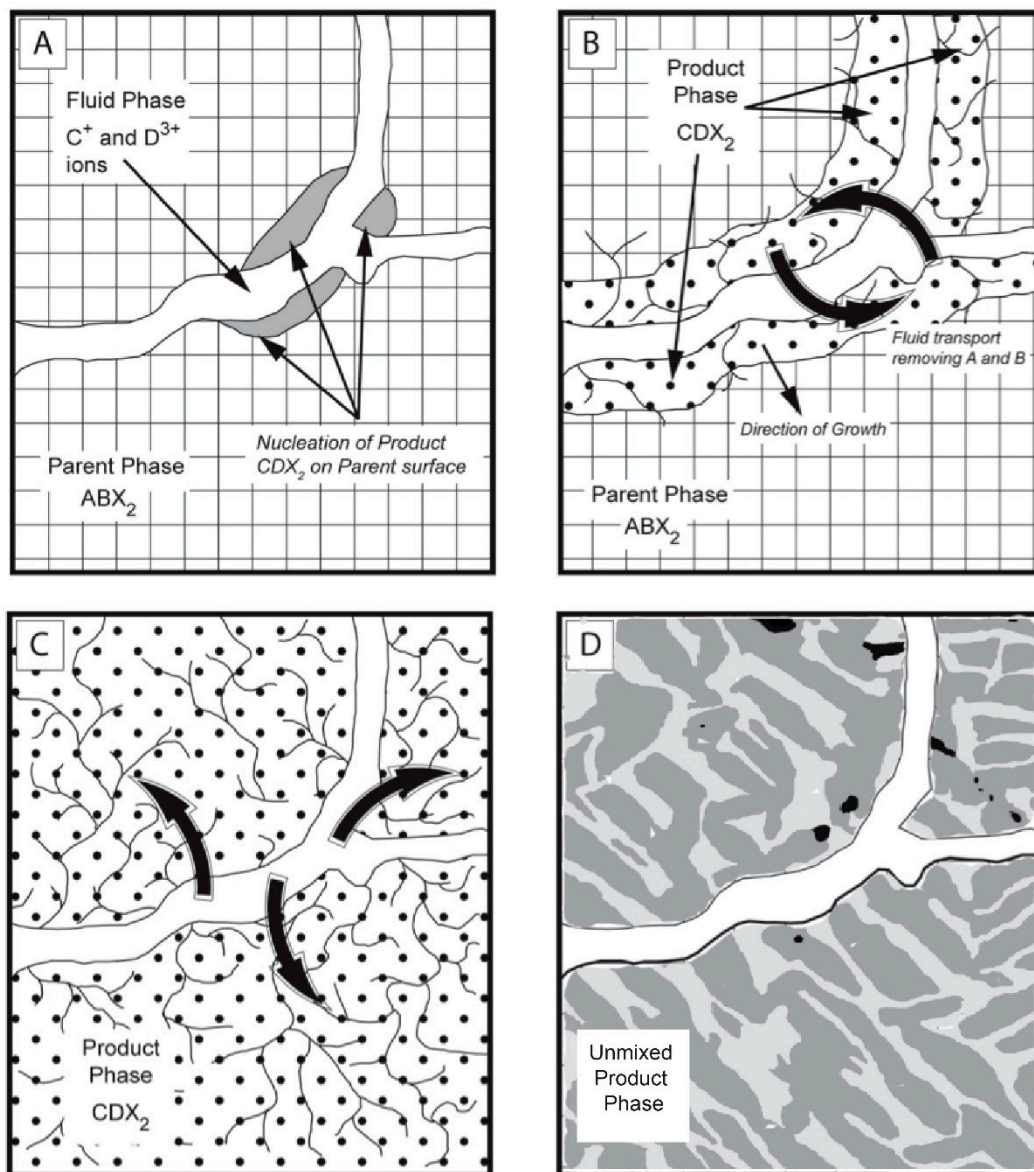
Figure 10. A diagrammatic representation of interface-coupled dissolution–reprecipitation. (**A**) Fluid containing C^+ and D^{3+} ions goes through cracks within the parent phase of ABX_2. ABX_2 phase dissolves at the reaction surface and CDX_2 product forms on the surface. (**B**) Fluid transports through pores and cracks to reaction interface adding C^+ and D^{3+}. (**C**) Curved arrows show direction of fluid flow. (**D**) Porosity anneals out over time and fluid inclusions form from the solution trapped within the crystal. Unstable product phase of CDX_2 exsolves into two new phases upon quenching, catalyzed by the fluid within the porosity and along the grain boundaries.

Table 2. Summary of experimental replacement reactions of gold–(silver) tellurides under hydrothermal conditions.

Parent Mineral	Average Composition	Au:Ag:Te	Overall Reaction	Mechanism	Products	ΔVm *
Calaverite	$Au_{0.94}Ag_{0.05}Te_{2.00}$	47:2.5:100	Calaverite + 2 O_2(aq) + 2 H_2O → Au + 2 H_2TeO_3(aq)	CDR	Porous gold	−79.32%
Sylvanite	$Au_{0.63}Ag_{0.36}Te_{2.00}$	31.5:17.75:100	Sylvanite + 2.07 O_2(aq) + 1.87 H_2O + 0.27 H^+(aq) + 0.27 Cl^- → 0.72 $Au_{0.87}Ag_{0.13}$ + 0.27 AgCl(aq) + 2 H_2TeO_3(aq)	CDR + exsolution	Porous Au–Ag alloy, $Au_{0.87}Ag_{0.13}$ Petzite, $(Au_{0.92}Ag_{3.15})Te_2$ Hessite, $Ag_{1.89}Au_{0.07}Te$ Calaverite I, $(Au_{0.78}Ag_{0.22})Te_{1.74}$ Calaverite II, $(Au_{0.93}Ag_{0.07})Te_2$	−84.92%
Krennerite	$Au_{0.82}Ag_{0.18}Te_{2.00}$	41:9:100	Krennerite + 2.01 O_2(aq) + 1.98 H_2O + 0.04 H^+(aq) + 0.04 Cl^- → 0.96 $Au_{0.85}Ag_{0.15}$ + 0.04 AgCl(aq) + 2 H_2TeO_3(aq)	CDR	Porous Au–Ag alloy, $Au_{0.85}Ag_{0.15}$	−80.19%

Note: * Volume change for each reaction was calculated using the Equation $\Delta V = 100 \cdot \left(\frac{n_p V_{m,p} - n_d V_{m,d}}{n_d V_{m,d}} \right)$, where n_p and n_d are the number of moles of product precipitated and parent dissolved, and $V_{m,p}$ and $V_{m,d}$ are the molar volumes of the precipitating and dissolving phases [46]. Molar volume of each phase equals the molar mass (M) divided by the mass density (ρ). The density of the starting minerals is listed in Table 1, and the average density of sylvanite is 8.1 g/cm^3. The density of gold–silver alloy was calculated using the data of gold density (19.32 g/cm^3) and silver density (10.49 g/cm^3). The calculated density of $Au_{0.87}Ag_{0.13}$ alloy is 17.41 g/cm^3 and 17.15 g/cm^3 for $Au_{0.85}Ag_{0.15}$.

4. Applications and Implications

The morphology of the nanoscale spongy gold wire produced by the replacement of calaverite under hydrothermal conditions is remarkably similar to the mustard gold samples [24,25] and the microporous gold samples [30] found in nature (Figure 11). Although the fluids used in the experiments are probably more aggressive than those found in nature, the similarity in the textures of porous gold may reflect similar processes of formation. The natural microporous gold found at the Aginskoe deposit, Central Kamchatka epithermal district [30], has remarkably similar textures to these synthetic spongy gold filaments in terms of both morphology and size. As shown in Figure 11, each grain of microporous gold from Aginskoe consists of aggregates of fine fibers that are about 30–300 nm in diameter and $\geq$5 µm in length. Andreeva et al. [27] indicated calaverite is the main Au telluride at Aginskoe and it is a likely precursor in this case. It often displays partial alteration to porous gold. The mustard gold found at the Dongping Mines (Hebei Province, China) is microporous gold aggregate [24] with slightly coarser textures. Mustard gold typically has the same Au:Ag ratio as the calaverite in the deposit, and the formation corresponds to the selective leaching of tellurium from calaverite. The recrystallization of gold may occur during or after the decomposition of calaverite, resulting in porous gold filaments. The textures of an ICDR product are normally related to the chemistry of the fluid, as demonstrated in the replacement of leucite ($KAlSi_2O_6$) by analcime ($NaAlSi_2O_6 \cdot H_2O$) [51]. The coarsening of the structure may also occur upon the completion of the replacement reaction, which is driven by surface energy reduction to create self-similar microstructures with ever-increasing filament size.
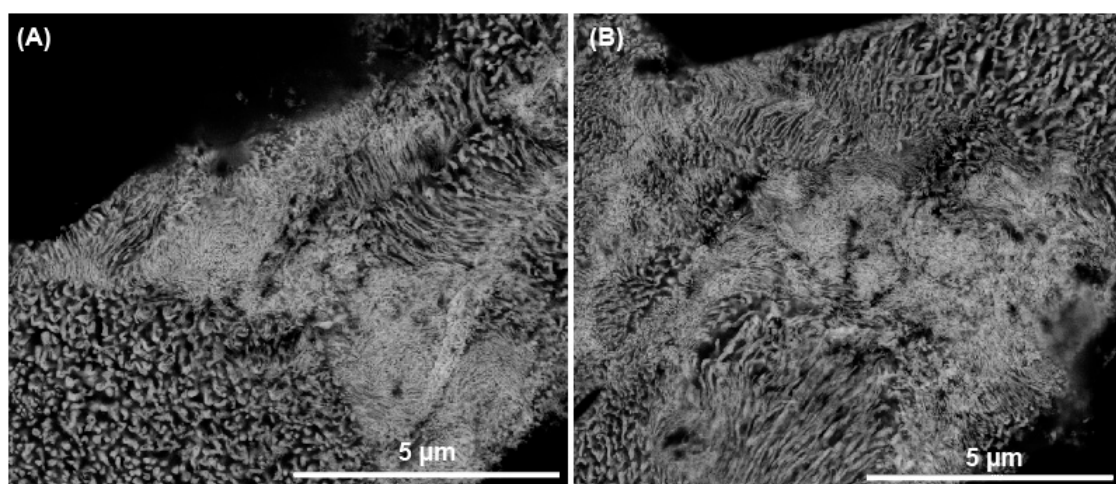

Figure 11. The natural microporous gold found at the Aginskoe deposit, Central Kamchatka epithermal district (imaged by Barbara Etschmann). (**A,B**) Microporous gold grain consists of aggregates of small fibers. The diameters of the gold fibers vary in a single grain.

The increasing knowledge base of the controls of interface-coupled dissolution–reprecipitation reactions over recent years is leading to an improved understanding of mineralization processes of natural systems. As shown in Figure 3, the typical textures of gold–(silver) tellurides from the Sandaowanzi gold deposit are krennerite–gold intergrowths imbedded within stuetzite–petzite symplectites. Here, the natural krennerite has a similar composition to synthetic calaverite I, and the composition of stuetzite is similar to that of synthetic hessite. According to the calculated bulk composition of the complex texture in Figure 3A, the precursor composition might have been a more Ag-rich but Te-depleted sylvanite than that used by Zhao et al. [16]. The complex textures observed at the Sandaowanzi deposit are remarkably similar to those synthesized (Figure 9) by Zhao et al. [16] by replacing sylvanite under hydrothermal conditions, implying broad similarities in the formation conditions. The experimental studies on the replacement of sylvanite by gold [17] indicate that the formation of the two/three-phase symplectites at Sandaowanzi gold deposit, are related to the

replacement of the gold–(silver) telluride precursor via an interface-coupled dissolution–reprecipitation. The precursor of the mineralization was formed by the upwelling of early mineralization fluids from a deep sub-alkaline magmatic source and the mineral precipitation at the near-surface faulting during the cooling [7,8]. The precursor reacts with meteoric water infiltrating within fractures along the quartz boundaries at mild temperatures, leading to the formation of gold, the precipitation of different gold–(silver) telluride mineral associations, and the different types of solid solutions (e.g., phase χ). The results of sylvanite replacement reaction directly explain the generation sequence of gold–(silver) tellurides in nature. Native gold, Au–Ag tellurides, and Ag tellurides at Sandaowanzi deposit are all the products of precursor replacement reactions, which were formed at the same time-scale but distributed in different layers of quartz matrix formed at different stages. The results also explain that some of the later mineral assemblages (e.g., hessite–petzite and stuetzite–petzite) represent the breakdown of metastable solid solutions during cooling rather than the initial reaction conditions of ore formation. In the experiments, the products are layered by the sequence of the reactions. From the surface of the sylvanite grain to the core, the layers of products show a general trend of increasing Ag telluride abundances together with a decrease in the abundance of Au-dominant tellurides. At the Sandaowanzi gold deposit, the high-grade vein ores are mainly distributed at the +130 m level, which is in the center of two low-grade disseminated mineralization zones along the margins of the orebody. According to the experimental results, the +130 m level could be the starting surface of reaction. The majority of the Te and Ag were dissolved into solution during alteration processes and transferred to the low-grade disseminated mineralization zone by fluids, eventually forming small particles of silver tellurides and other tellurides (e.g., HgTe and PbTe) within the matrix of very fine-grained quartz (μm scale).

The recent studies on gold–(silver) tellurides under hydrothermal conditions show that these minerals can be transformed to gold/Au–Ag alloy relatively rapidly (within hours) under all conditions (even in Milli-Q water) at moderately elevated temperatures (~200 °C). This process could be added as a preliminary treatment in ore processing before the traditional cyanide process. For gold-bearing tellurides, the overall reactions provide an efficient and less toxic alternative to pretreatment by roasting.

5. Outlook

Porous gold is a form of gold with significant technological potential due to its low density, high strength and large specific surface area. The dramatic increase in attention to this material over the last two decades is due to its many potential applications in areas such as catalysis, energy storage, and sensor technology. A number of methods for synthesizing this material have been developed—for example, de-alloying, templating, electrochemical, and self-assembling. De-alloying of gold metal alloys is currently the most widely-used method. This approach fabricates the porous gold structure by selectively dissolving the less noble components from a gold alloy. To make a porous gold sponge by de-alloying, Au–Ag alloy is firstly synthesized and then the Au–Ag alloy is treated with a high-concentration nitrate solution [52]. This is a two-step process, excluding any purification of the gold source. However, a similar structure of porous gold can be produced by replacing natural gold–(silver) tellurides using a hydrothermal method over a wide range of solutions under mild conditions, the reaction being completed within days, depending on the solution composition. This single-step method appears to have the advantage of allowing fine-tuning of the nature of the porous gold, as the dissolution of a gold telluride occurs over a much wider range of solution conditions than does that of a simple Au–Ag alloy. It is also possible to use natural gold telluride minerals as well as synthetic gold tellurides. A comprehensive experimental study of the controls on the texture of the porous gold obtained via such a route is required to optimize the reaction conditions, manipulate the morphology of the porous gold sponge, and test this porous gold as a functional material in terms of catalysis, energy storage, and sensor technology.

References

1. Shackleton, J.M.; Spry, P.G.; Bateman, R. Telluride mineralogy of the Golden Mile deposit, Kalgoorlie, Western Australia. *Can. Miner.* **2003**, *41*, 1503–1524. [CrossRef]

2. Kelley, K.D.; Romberger, S.B.; Beaty, D.W.; Pontius, J.A.; Snee, L.W.; Stein, H.J.; Thompson, T.B. Geochemical and geochronological constraints on the genesis of Au-Te deposits at Cripple Creek, Colorado. *Econ. Geol.* **1998**, *93*, 981–1012. [CrossRef]

3. Ahmad, M.; Solomon, M.; Walshe, J.L. Mineralogical and geochemical studies of the Emperor gold telluride deposit, Fiji. *Econ. Geol.* **1987**, *82*, 234–270. [CrossRef]

4. Cook, N.J.; Ciobanu, C.L.; Spry, P.G.; Voudouris, P.; the participants of IGCP-486. Understanding gold-(silver)-telluride-(selenide) mineral deposits. *Episodes* **2009**, *32*, 249–263.

5. Cook, N.J.; Ciobanu, C.L.; Capraru, N.; Damian, G.; Cristea, P. Mineral assemblages from the vein salband at Sacarimb, Golden Quadrilateral, Romania: II. Tellurides. *Geochem. Miner. Petrol.* **2005**, *43*, 56–63.

6. Tran, M.D.; Liu, J.L.; Hu, J.J.; Zou, Y.X.; Zhang, H.Y. Discovery and geological significance of Sandaowanzi telluride type gold deposit in the northern Daxing'anling, Heilongjiang, China. *Geol. Bull. China* **2008**, *27*, 584–589.

7. Liu, J.L.; Bai, X.D.; Zhao, S.J.; Tran, M.D.; Zhang, Z.C.; Zhao, Z.D.; Zhao, H.B.; Lu, J. Geology of the Sandaowanzi telluride gold deposit of the northern Great Xing'an Range, NE China: Geochronology and tectonic controls. *J. Asian Earth Sci.* **2011**, *41*, 107–118. [CrossRef]

8. Liu, J.L.; Zhao, S.J.; Cook, N.J.; Bai, X.D.; Zhang, Z.C.; Zhao, Z.D.; Zhao, H.B.; Lu, J. Bonanza-grade accumulations of gold tellurides in the Early Cretaceous Sandaowanzi deposit, northeast China. *Ore Geol. Rev.* **2013**, *54*, 110–126. [CrossRef]

9. Zhai, D.; Liu, J. Gold-telluride-sulfide association in the Sandaowanzi epithermal Au-Ag-Te deposit, NE China: Implications for phase equilibrium and physicochemical conditions. *Miner. Petrol.* **2014**, *108*, 853–871. [CrossRef]

10. Cabri, L.J. Phase relations in the Au-Ag-Te system and their mineralogical significance. *Econ. Geol.* **1965**, *60*, 1569–1605. [CrossRef]

11. Bindi, L.; Arakcheeva, A.; Chapuis, G. The role of silver on the stabilization of the incommensurately modulated structure in calaverite, $AuTe_2$. *Am. Miner.* **2009**, *94*, 728–736. [CrossRef]

12. Dye, M.D.; Smyth, J.R. The crystal structure and genesis of krennerite, Au_3AgTe_8. *Can. Miner.* **2012**, *50*, 363–371. [CrossRef]

13. Van Tendeloo, G.; Amelinckx, S.; Gregoriades, P. Electron microscopic studies of modulated structures in $(Au, Ag) Te_2$: III. Krennerite. *J. Solid State Chem.* **1984**, *53*, 281–289. [CrossRef]

14. Smith, G.F.H. On the remarkable problem presented by crystalline development of calaverite. *Miner. Mag.* **1901**, *13*, 122–150.

15. Mineral Database. Available online: http://webmineral.com/data/ (accessed on 8 March 2019).

16. Zhao, J.; Xia, F.; Pring, A.; Brugger, J.; Grundler, P.V.; Chen, G. A novel pre-treatment of calaverite by hydrothermal mineral replacement reactions. *Miner. Eng.* **2010**, *23*, 451–453. [CrossRef]

17. Zhao, J.; Brugger, J.; Xia, F.; Ngothai, Y.; Chen, G.; Pring, A. Dissolution-reprecipitation vs. solid-state diffusion: Mechanism of mineral transformations in sylvanite, $(AuAg)_2Te_4$, under hydrothermal conditions. *Am. Miner.* **2013**, *98*, 19–32. [CrossRef]

18. Kongolo, K.; Mwema, M.D. The extractive metallurgy of gold. *Hyperfine Interact.* **1998**, *111*, 281–289. [CrossRef]

19. Grosse, A.C.; Dicinoski, G.W.; Shaw, M.J.; Haddad, P.R. Leaching and recovery of gold using ammoniacal thiosulfate leach liquors (a review). *Hydrometallurgy* **2003**, *69*, 1–21. [CrossRef]

20. Hodge, A.M.; Hayes, J.R.; Caro, J.A.; Biener, J.; Hamza, A.V. Characterization and Mechanical Behavior of Nanoporous Gold. *Adv. Eng. Mater.* **2006**, *8*, 853–857. [CrossRef]

21. Ciobanu, C.L.; Cook, N.J.; Damian, G.H.; Damian, F.L.; Buia, G. Telluride and sulphosalt associations at Scrâmb. In *Gold-Silver-Telluride Deposits of the Golden Quadrilateral, South Apuseni Mts*; IAGOD: Alba Iulia, Romania, 2004; Volume 12, pp. 145–186.

22. Wilson, A.F. Origin of quartz-free gold nuggets and supergene gold found in laterites and soils—A review and some new observations. *Aust. J. Earth Sci.* **1984**, *31*, 303–316.

23. Tolstykh, N.; Vymazalova, A.; Tuhy, M.; Shapovalova, M. Conditions of formation of Au-Se-Te mineralization in the Gaching ore occurrence (Maletoyvayam ore field), Kamchatka, Russia. *Miner. Mag.* **2018**, *82*, 649–674. [CrossRef]

24. Petersen, S.B.; Makovicky, E.; Li, J.L.; Rose-Hansen, J. Mustard gold from the Dongping Au–Te deposit, Hebei Province, People's Republic of China. *Neues Jahrb. Mineral. Mon.* **1999**, *8*, 337–357.

25. Li, J.L.; Makovicky, E. New studies on mustard gold from the Dongping Mines, Hebei Province, China: The tellurian, plumbian, manganoan, and mixed varieties. *Neues Jahrb. Mineral. Abh.* **2001**, *176*, 269–297.

26. Palache, C.; Berman, H.; Frondel, C. *Dana's System of Mineralogy I*; Wiley: New York, NY, USA, 1944.

27. Andreeva, E.D.; Matsueda, H.; Okrugin, V.M.; Takahashi, R.; Ono, S. Au–Ag–Te mineralization of the low-sulfidation epithermal Aginskoe deposit, Central Kamchatka, Russia. *Resour. Geol.* **2013**, *63*, 337–349. [CrossRef]

28. Zhao, J.; Brugger, J.; Grundler, P.V.; Xia, F.; Chen, G.; Pring, A. Mechanism and kinetics of a mineral transformation under hydrothermal conditions: Calaverite to metallic gold. *Am. Miner.* **2009**, *94*, 1541–1555. [CrossRef]

29. Xu, W.; Zhao, J.; Brugger, J.; Chen, G.; Pring, A. Mechanism of mineral transformations in krennerite, Au_3AgTe_8, under hydrothermal conditions. *Am. Miner.* **2013**, *98*, 2086–2095. [CrossRef]

30. Okrugin, V.M.; Andreeva, E.; Etschmann, B.; Pring, A.; Li, K.; Zhao, J.; Griffiths, G.; Lumpkin, G.R.; Triani, G.; Brugger, J. Microporous gold: Comparison of textures from Nature and experiments. *Am. Miner.* **2014**, *99*, 1171–1174. [CrossRef]

31. Markham, W.L. Synthetic and natural phases in the system Au–Ag–Te, Part 1 and 2. *Econ. Geol.* **1960**, *55*, 1148–1178. [CrossRef]

32. Legendre, B.; Souleau, C.; Hancheng, C. Le système ternaire or-argent-tellure. *Bulletin de al Société Chimique de France Partie* **1980**, *1*, 197–204. (In French)

33. Afifi, A.M.; Kelly, W.C.; Essene, E.J. Phase relations among tellurides, sulfides, and oxides: I. Thermochemical data and calculated equilibria; II. Applications to telluride-bearing ore deposits. *Econ. Geol.* **1988**, *83*, 377–394. [CrossRef]

34. Zhang, X.; Spry, P.G. Petrological, mineralogical, fluid inclusion, and stable isotope studies of the Gies gold-silver telluride deposit, Judith Mountains, Montana. *Econ. Geol.* **1994**, *89*, 602–627. [CrossRef]

35. Wang, J.H.; Lu, X.G.; Sundman, B.; Su, X.P. Thermodynamic reassessment of the Au-Te system. *J. Alloys Compd.* **2006**, *407*, 106–111. [CrossRef]

36. McPhail, D.C. Thermodynamic properties of aqueous tellurium species between 25 and 350 °C. *Geochim. Cosmochim. Acta* **1995**, *59*, 851–866.

37. Grundler, P.V.; Brugger, J.; Meisser, N.; Ansermet, S.; Borg, S.; Etschmann, B.; Testemale, D.; Bolin, T. Xocolatlite, $Ca_2Mn_2^{4+}Te_2O_{12}·H_2O$, a new tellurate related to kuranakhite: Description and measurement of Te oxidation state by XANES spectroscopy. *Am. Miner.* **2008**, *93*, 1911–1920. [CrossRef]

38. Grundler, P.V.; Pring, A.; Brugger, J.; Spry, P.G.; Helm, L. Aqueous solubility and speciation of Te(IV) at elevated temperatures. *Geochim. Cosmochim. Acta* **2009**, *73*, A472.

39. Grundler, P.V.; Brugger, J.; Etschmann, B.E.; Helm, L.; Liu, W.; Spry, P.G.; Tian, Y.; Testemale, D.; Pring, A. Speciation of aqueous tellurium(IV) in hydrothermal solutions and vapors, and the role of oxidized tellurium species in Te transport and gold deposition. *Geochim. Cosmochim. Acta* **2013**, *120*, 298–325. [CrossRef]

40. Putnis, A. Mineral replacement reactions. *Rev. Mineral. Geochem.* **2009**, *70*, 87–124. [CrossRef]

41. Putnis, A.; Austrheim, H. Mechanisms of metasomatism and metamorphism on the local mineral scale: The role of dissolution-reprecipitation during mineral reequilibration. In *Metasomatism and the Chemical Transformation of Rock*; Harlov, D.E., Austrheim, H., Eds.; Springer: Berlin, Germany, 2013.

42. Altree-Williams, A.; Pring, A.; Ngothai, Y.; Brugger, J. Textural and compositional complexities resulting from coupled dissolution-reprecipitation reactions in geomaterials. *Earth Sci. Rev.* **2015**, *150*, 628–651. [CrossRef]

43. Putnis, A.; Putnis, C.V. The mechanism of reequilibration of solids in the presence of a fluid phase. *J. Solid State Chem.* **2007**, *180*, 1783–1786. [CrossRef]

44. Xia, F.; Brugger, J.; Chen, G.; Ngothai, Y.; O'Neill, B.; Putnis, A.; Pring, A. Mechanism and kinetics of pseudomorphic mineral replacement reactions: A case study of the replacement of pentlandite by violarite. *Geochim. Cosmochim. Acta* **2009**, *73*, 1945–1969. [CrossRef]

45. Zhao, J.; Brugger, J.; Chen, G.; Ngothai, Y.; Pring, A. Experimental study of the formation of chalcopyrite and bornite via the sulfidation of hematite: Mineral replacements with a large volume increase. *Am. Miner.* **2014**, *99*, 343–354. [CrossRef]

46. Pollok, K.; Putnis, C.V.; Putnis, A. Mineral replacement reactions in solid solution-aqueous solution systems: Volume changes, reactions paths and end-points using the example of model salt systems. *Am. J. Sci.* **2011**, *311*, 211–236. [CrossRef]

47. Ruiz-Agudo, E.; Putnis, C.V.; Putnis, A. Coupled dissolution and precipitation at mineral-fluid interfaces. *Chem. Geol.* **2014**, *383*, 132–146. [CrossRef]

48. Zhao, J.; Brugger, J.; Grguric, B.A.; Ngothai, Y.; Pring, A. Fluid enhanced coarsening of mineral microstructures in hydrothermally synthesized bornite-digenite solid solution. *ACS Earth Space Chem.* **2017**, *1*, 465–474. [CrossRef]

49. Li, K.; Brugger, J.; Pring, A. Exsolution of chalcopyrite from bornite-digenite solid solution: An example of a fluid-driven back-replacement reaction. *Miner. Depos.* **2018**, *53*, 903–908. [CrossRef]

50. Zhao, J.; Brugger, J.; Ngothai, Y.; Pring, A. The replacement of chalcopyrite by bornite under hydrothermal conditions. *Am. Miner.* **2014**, *99*, 2389–2397. [CrossRef]

51. Xia, F.; Brugger, J.; Ngothai, Y.; O'Neill, B.; Chen, G.; Pring, A. Three-dimensional ordered arrays of zeolite nanocrystals with uniform size and orientation by a pseudomorphic coupled dissolution-reprecipitation replacement route. *Cryst. Growth Des.* **2009**, *9*, 4902–4906. [CrossRef]

52. Pertlik, F. Kristallchemie natürlicher Telluride I: Verfeinerung der Kristallstruktur des Sylvanits; $AuAgTe_4$. *Tschermaks Mineralogische und Petrographische Mitteilungen* **1984**, *33*, 203–212. (In German) [CrossRef]